

Paper

Quantitative attractor analysis of high-capacity kernel Hopfield networks

Akira Tamamori  ¹¹ Aichi Institute of Technology, Aichi, 470-0392, Japan.

Received October 27, 20XX; Revised December 29, 20XX; Published July 1, 20XX

Abstract: Kernel-based learning methods such as Kernel Logistic Regression (KLR) can substantially increase the storage capacity of Hopfield networks, but the principles governing their performance and stability remain largely uncharacterized. This paper presents a comprehensive quantitative analysis of the attractor landscape in KLR-trained networks to establish a solid foundation for their design and application. Through extensive, statistically validated simulations, we address critical questions of generality, scalability, and robustness. Our comparative analysis shows that KLR and Kernel Ridge Regression (KRR) exhibit similarly high storage capacities and clean attractor landscapes under typical operating conditions, suggesting that this behavior is a general property of kernel regression methods, although KRR is computationally much faster. We identify a non-trivial, scale-dependent law for the kernel width γ , demonstrating that optimal capacity requires γ to be scaled such that γN increases with network size N . This finding implies that larger networks require more localized kernels, in which each pattern's influence is more spatially confined, to mitigate inter-pattern interference. Under this optimized scaling, we provide clear evidence that storage capacity scales linearly with network size ($P \propto N$). Furthermore, our sensitivity analysis shows that performance is remarkably robust with respect to the choice of the regularization parameter λ . Collectively, these findings provide a concise set of empirical principles for designing high-capacity and robust associative memories and clarify the mechanisms that enable kernel methods to overcome the classical limitations of Hopfield-type models.

Key Words: Hopfield network, Kernel logistic regression, Associative memory, Storage capacity, Noise robustness, Attractor analysis

1. Introduction

Associative memory (AM) is a fundamental cognitive function that enables the retrieval of stored information based on partial or noisy cues. Artificial neural networks, particularly the Hopfield network [1], have long served as foundational models for AM due to their biologically plausible recurrent dynamics and the interpretation of stored memories as stable states (attractors) of an energy function. The recall process in a Hopfield network can be viewed as the network state evolving toward a local minimum of its energy landscape, corresponding to the stored pattern that is most similar to the input cue.

Despite their conceptual elegance and biological grounding, traditional Hopfield networks trained with the Hebbian learning rule [1] exhibit severe limitations. Their storage capacity is theoretically bounded at a pattern-to-neuron ratio (P/N) of approximately 0.14 [2]. Exceeding this limit leads to catastrophic interference, recall errors, and the proliferation of *spurious attractors*, which do not correspond to any learned pattern yet still act



as fixed points of the network dynamics [3]. These spurious attractors compete with desired memories, reduce their basins of attraction, and significantly impair noise robustness.

To overcome these limitations, several approaches have reframed associative memory learning as a supervised optimization problem in which synaptic weights are tuned to make desired patterns stable fixed points. Linear methods, such as the pseudoinverse rule [4] and Linear Logistic Regression (LLR) [5], provide moderate improvements in storage capacity and robustness. However, their performance remains fundamentally constrained by the requirement of linear separability, either in the input space or in the neuron’s input–output mapping.

Nonlinear kernel methods offer a powerful means to transcend these constraints. Techniques such as Support Vector Machines (SVMs), Kernel Ridge Regression (KRR), and Kernel Logistic Regression (KLR) implicitly map data into high- or even infinite-dimensional feature spaces, where complex nonlinear relationships become linearly separable [6]. Applying this framework to associative memory learning holds the potential to dramatically increase storage capacity and enhance noise robustness.

Our previous work [7] revealed the remarkable potential of KLR for training high-capacity Hopfield networks, demonstrating storage capacities far exceeding the classical limit. This initial discovery, however, left fundamental questions regarding the generality, scalability, and robustness of this approach unanswered. For instance, is the choice of the loss function critical? How does performance scale with network size N ? And which hyperparameters govern the stability?

This paper aims to answer these questions through a comprehensive quantitative analysis. We systematically investigate the attractor landscape by conducting a series of rigorous, statistically validated experiments, including (1) a direct comparison with KRR, (2) a multi-scale analysis of storage capacity, and (3) a detailed hyperparameter sensitivity study.

The main contributions of this work are as follows:

1. We confirm and statistically validate that KLR-trained networks achieve significantly higher storage capacity and noise robustness, exhibiting a remarkably clean attractor landscape, nearly devoid of spurious states under typical noise conditions.
2. We reveal that KLR and KRR exhibit qualitatively similar recall performance, suggesting that the high-capacity nature is a general property of kernel regression methods in this context. However, KRR holds a significant advantage in computational speed.
3. We uncover a non-trivial scaling law for the kernel width γ , demonstrating that optimal capacity is achieved when γ is scaled appropriately with N . Under these optimized conditions, we confirm that the storage capacity P scales linearly with N .
4. We show that the network’s high performance is robust across a reasonable range of hyperparameter values.

These findings offer deep insights into how kernel-based learning reshapes the dynamical system of a Hopfield network to create a highly effective associative memory. By moving beyond the initial discovery of high performance to a deeper characterization of its generality, scaling properties, and robustness, this work establishes a solid foundation for the design and application of high-capacity, Hopfield-type models.

2. Related Work

Traditional approaches to Hopfield network learning, primarily relying on Hebbian rules, suffer from limited storage capacity [1, 2] and the emergence of spurious attractors [3]. Linear learning methods, such as the pseudoinverse rule [4] and those based on Linear Logistic Regression (LLR) [5], offer some improvement but remain fundamentally constrained by the linear separability of stored patterns in the input space.

The application of nonlinear kernel methods to associative memory learning represents a promising direction. Kernel Associative Memories (KAM) [9] first proposed leveraging high-dimensional feature spaces to theoretically achieve vast storage capacities. Early theoretical analyses, such as those by Caputo and Niemann [10] using spin-glass theory, provided initial evidence that polynomial and Gaussian kernels could indeed yield a notable improvement over the classical Hopfield model.

More recently, the connection between Hopfield-type networks and modern deep learning architectures has revitalized the field. A landmark paper by Ramsauer et al. [11] demonstrated that the attention mechanism in Transformers can be interpreted as a modern Hopfield network with a continuous state representation and an updated energy function. These Modern Hopfield Networks (MHNs) have shown immense storage capacities, scaling polynomially or even exponentially with the feature dimension. This work firmly positions the study of Hopfield-like energy-based models at the heart of current AI research.

While these important lines of research, ranging from classical KAM to MHNs, have demonstrated the potential for high-capacity associative memory, their focus has primarily been on the static properties of the energy function or on performance in specific pattern reconstruction tasks. A detailed and quantitative understanding of the attractor landscape and recall dynamics that arise from practical supervised kernel methods such as KLR and KRR remains largely unexplored. Key questions persist: What happens to spurious attractors in these high-capacity regimes? What are the primary failure modes of recall? What are the geometric properties of the attractors themselves?

The present study aims to address this gap. We connect the high-level capacity analysis of KAM and MHN with the classical dynamical systems perspective on Hopfield networks. By conducting a detailed quantitative analysis of the attractor landscape formed by KLR and comparing it with KRR, for which we have separately demonstrated strong performance and computational advantages [8], we provide a microscopic and dynamical explanation of how these kernel-based methods achieve their notable performance, thereby complementing the existing body of research.

3. Model and Methods

3.1 Network Model

We consider a standard Hopfield network composed of N fully connected bipolar neurons, with states $s_i \in \{-1, 1\}$ for $i = 1, \dots, N$. The network evolves over discrete time steps. Given a state $s(t)$ at time t , the next state $s(t+1)$ is determined by updating each neuron based on its activation potential.

3.2 Learning Algorithms for Comparison

For comparison, we briefly describe the conventional Hebbian learning rule and Linear Logistic Regression (LLR), as implemented in our previous work [7].

3.2.1 Hebbian Learning

The Hebbian learning rule defines the synaptic weights W_{ij} based on correlations between the activities of neurons i and j across P stored patterns $\{\xi^\mu\}_{\mu=1}^P$:

$$W_{ij} = \frac{1}{N} \sum_{\mu=1}^P \xi_i^\mu \xi_j^\mu, \quad (i \neq j), \quad W_{ii} = 0. \quad (1)$$

Recall is performed using standard linear threshold dynamics:

$$s_i(t+1) = \text{sign} \left(\sum_{j \neq i} W_{ij} s_j(t) \right), \quad (2)$$

where $\text{sign}(z) = 1$ if $z \geq 0$ and -1 if $z < 0$.

3.2.2 Linear Logistic Regression (LLR)

In the LLR approach [5], learning for each neuron i is formulated as predicting ξ_i^μ from the remaining neuron states $\xi_{j \neq i}^\mu$. A linear logistic regression model is trained for each neuron to obtain a weight vector w_i . The logit for neuron i given a network state s is computed as $h_i(s) = \sum_{j \neq i} W_{ij} s_j$. The weights are optimized by minimizing a regularized negative log-likelihood using gradient descent. After training, the resulting $N \times N$ symmetric weight matrix W_{ij} is used for recall with the same dynamics as Hebbian learning.

3.2.3 Kernel Logistic Regression (KLR) Hopfield Network

The primary focus of this work is the Hopfield network trained using Kernel Logistic Regression (KLR), as proposed in our previous study [7]. KLR treats the learning for each neuron i as an independent binary classification task, predicting the target state $t_i^\mu = (\xi_i^\mu + 1)/2 \in \{0, 1\}$ from the input pattern $\xi^\mu \in \{-1, 1\}^N$.

KLR employs the kernel trick [6] to implicitly map input patterns into a high-dimensional feature space. The logit for neuron i given a pattern ξ is computed as a weighted sum of kernel similarities to the stored patterns:

$$h_i(\xi) = \sum_{\mu=1}^P \alpha_{\mu i} K(\xi, \xi^\mu). \quad (3)$$

We adopt the Radial Basis Function (RBF) kernel $K(\mathbf{x}, \mathbf{y}) = \exp(-\gamma \|\mathbf{x} - \mathbf{y}\|^2)$, which measures pairwise similarity between patterns in the feature space. The dual variables $\alpha_i = [\alpha_{1i}, \dots, \alpha_{Pi}]^T$ for each neuron i are learned by minimizing the L2-regularized negative log-likelihood objective function. The objective function (loss function) L_i to be minimized for neuron i is given by:

$$L_i(\alpha_i) = - \sum_{\mu=1}^P [t_i^\mu \log(\sigma(h_i(\xi^\mu))) + (1 - t_i^\mu) \log(1 - \sigma(h_i(\xi^\mu)))] + \frac{\lambda}{2} \alpha_i^\top \mathbf{K} \alpha_i, \quad (4)$$

$h_i(\xi^\mu)$ is the logit from Eq. (3), $\sigma(z) = 1/(1 + e^{-z})$ is the sigmoid function, and λ is the L2-regularization parameter. This optimization is performed via gradient descent.

3.2.4 Kernel Ridge Regression (KRR) Hopfield Network

As a key point of comparison, we also investigate networks trained with Kernel Ridge Regression (KRR) [8]. Like KLR, KRR is a kernel-based method that learns a set of dual variables, $\alpha \in \mathbb{R}^{P \times N}$. However, it differs from KLR in two fundamental aspects: the task formulation and the optimization procedure.

First, KRR frames the learning problem as a regression task rather than a classification task. The goal is to make the network's output $h_i(\cdot)$ directly approximate the target bipolar states $\{-1, 1\}^N$ by minimizing a squared error loss. The objective function for each neuron i is to minimize:

$$L_i(\alpha_i) = \sum_{\mu=1}^P (\xi_i^\mu - h_i(\xi^\mu))^2 + \frac{\lambda}{2} \alpha_i^\top \mathbf{K} \alpha_i. \quad (5)$$

Second, and most critically from a practical standpoint, this squared-error objective function leads to a closed-form, non-iterative solution for the dual variables α . The optimal α can be found directly by solving the following system of linear equations:

$$(\mathbf{K} + \lambda \mathbf{I})\alpha = \mathbf{Y}, \quad (6)$$

where \mathbf{K} is the $P \times P$ kernel (Gram) matrix $K_{\mu\nu} = K(\xi^\mu, \xi^\nu)$, \mathbf{I} is the identity matrix, and \mathbf{Y} is the $P \times N$ matrix of stored patterns. This non-iterative solution makes the training process of KRR significantly faster than the gradient-based optimization required for KLR, a difference we quantify in our experiments.

Once α is learned, the recall dynamics are identical to those of the KLR network, as described in Section 3.4.

3.3 Lyapunov Function Candidate for Landscape Analysis

To provide a theoretical framework for analyzing the attractor landscape, we define a Lyapunov function candidate for the KLR network dynamics. While the synchronous update rule of the KLR network does not guarantee the monotonic decrease of a traditional energy function, we can define a scalar function $V(\mathbf{s})$ whose landscape geometry reflects the restorative forces of the system. We define this function as:

$$V(\mathbf{s}) = - \sum_{k=1}^N s_k h_k(\mathbf{s}), \quad (7)$$

where $h_k(\mathbf{s})$ is the input potential to neuron k as defined in Eq. (3). This function measures the total alignment between the neuron states s_k and their corresponding input potentials $h_k(\mathbf{s})$. A lower value of $V(\mathbf{s})$ indicates a

state that is more consistent with the dynamics of the network; thus, the network’s dynamics can be viewed as a process that seeks to find local minima of this function $V(s)$.

The local stability of an attractor ξ^μ can then be characterized by the steepness of the landscape of $V(s)$ in its vicinity. As will be detailed in our experimental analysis, the gradient of this function, $\nabla V(s)$, provides a powerful tool for quantitatively characterizing the properties of the attractor landscape. The primary scope of this paper is to use this tool for an empirical and phenomenological analysis of the landscape. A detailed theoretical investigation into the mathematical structure of $V(s)$ and its resulting phase diagram is the subject of our companion paper [12]. Therefore, this paper does not delve into the rigorous theoretical proofs of stability, but rather establishes the empirical foundations upon which such theories can be built.

3.4 Recall Process

The recall process in KLR-trained networks differs from that in Hebbian and LLR-based networks, as it does not rely on an explicit $N \times N$ weight matrix. Given a network state $s(t)$ at time t , the next state $s(t + 1)$ is determined by the sign of each neuron’s activation potential relative to a threshold θ :

$$s_i(t + 1) = \text{sign}(h_i(s(t)) - \theta_i), \quad (8)$$

where

$$h_i(s(t)) = \sum_{\mu=1}^P \alpha_{\mu i} K(s(t), \xi^\mu) \quad (9)$$

is the logit for neuron i . In this study, the threshold vector was set to $\theta = \mathbf{0}$, i.e., $\theta_i = 0$ for all i . The recall process involves computing kernel values between the current state and all P stored patterns at each iteration.

3.5 Experimental Setup

We conducted a series of large-scale numerical simulations to systematically analyze the attractor landscape and performance characteristics of kernel-based Hopfield networks. All simulations were implemented in Python 3.13 using the NumPy 2.1.3 and SciPy 1.15.2 libraries and were executed on a standard workstation equipped with an Intel Core i9-9900K CPU and 64 GB of RAM. No GPU acceleration was used.

3.5.1 Network and Learning Parameters

Unless otherwise specified, the network size was set to $N = 500$ for detailed attractor analysis and $N = 100$ for comparative and sensitivity analyses. Stored patterns ξ^μ were generated as random bipolar vectors $\{-1, 1\}^N$, with each element sampled independently with equal probability.

For the KLR learning process, we used gradient descent with a learning rate $\beta = 0.1$ and number of parameter updates $M = 200$. For the KRR learning process, the closed-form solution was used. The L2-regularization parameter λ was set to a default value of $\lambda = 0.01$ for most experiments, except for the sensitivity analysis. As shown in Appendix A, the learning curve for a challenging high-load condition ($N = 500$, $P/N = 4.0$) demonstrates that the loss substantially decreases within the initial ~ 150 steps and approaches a plateau, confirming that 200 updates are adequate to achieve a well-converged model.

The RBF kernel width γ is a critical parameter. A common heuristic for kernel methods is to scale the width inversely with the input dimension, such as $\gamma = 1/N$, to maintain a constant level of pattern similarity irrespective of N [6]. However, our preliminary analysis revealed that the optimal γ scales with N in a non-trivial manner. To determine these optimal, N -dependent values, we performed a simplified grid search. For each network size N (100, 250, 500), we tested several values of the scaling factor c in $\gamma = c/N$, where c ranged from 0.5 to 10.0. We evaluated the average Target Recall Rate across multiple high-load conditions (P/N from 1.5 to 4.0) with a fixed initial similarity of 1.0. This search revealed that the optimal factor c_{opt} increases with N (e.g., $c_{\text{opt}} \approx 2$ for $N \leq 250$ and $c_{\text{opt}} \approx 5$ for $N = 500$), indicating that larger networks require more localized kernels than the conventional heuristic suggests. Therefore, for the main experiments, we used these empirically determined optimal γ values to ensure a fair comparison across scales. The detailed results of this sensitivity are presented in Section 4.4.

3.5.2 Simulation Experiments

We designed four main sets of experiments to address the key questions of this study:

1. **Attractor Landscape Analysis** ($N = 500$): To characterize the detailed structure of the attractors, we evaluated recall dynamics across a wide range of storage loads (P/N from 0.05 to 4.0) and initial similarities (from 0.05 to 1.0).
2. **Comparative Analysis** (KLR vs. KRR, $N = 100$): To compare KLR with KRR, we measured their recall performance and training time under identical conditions, sweeping P/N from 0.1 to 6.0.
3. **Scaling Analysis**: To verify the capacity scaling law, we performed the capacity analysis for three different network sizes ($N = 100, 250, 500$) using their respective optimal gamma values.
4. **Hyperparameter Sensitivity Analysis** ($N = 100$): To assess the robustness of the model, we evaluated the recall performance while systematically varying the parameters γ (via c) and λ at fixed medium ($P/N = 1.5$) and high ($P/N = 3.0$) storage loads.

3.6 Attractor Analysis Methodology

3.6.1 Recall Simulation and Convergence Criteria

To ensure statistical reproducibility, all experiments were repeated across five different master random seeds. Each master seed determined the generation of stored patterns and the initialization of the learning process. Within each master seed trial, further randomization for initial state generation was controlled by separate seeds to ensure diverse sampling.

For each combination of P/N and initials similarity, five noisy initial states were generated for each of the P stored patterns, resulting in a total of $5 \times P$ recall trials per condition per master seed.

The recall dynamics were simulated for a maximum of 30 discrete, synchronous update steps. Convergence was classified into three categories:

- *Fixed Point*: The state remains unchanged for one consecutive step.
- *Limit Cycle*: The state returns to any previously visited state within the trial.
- *Not Converged*: Neither of the above occurs within the maximum steps.

3.6.2 Classification of Final States

Once a trial converges, we further analyze the nature of the final state s_{final} to characterize the attractor landscape. Each final state s_{final} reached in a recall trial was classified into one of the following categories based on strict equality checks against the P stored patterns:

- *Target Pattern*: s_{final} is identical to the original target pattern ξ^ν from which the initial state was generated.
- *Other Learned Pattern*: s_{final} is identical to one of the other $P - 1$ learned patterns (ξ^ν where $\mu \neq \nu$).
- *Spurious Attractor*: s_{final} is a fixed point or a limit cycle state that is not identical to any of the P learned patterns.

The validity of this strict, equality-based classification is supported by the distribution of Hamming distances between final states and their nearest learned patterns. As detailed in Appendix B, this analysis confirms a clear separation, with no spurious attractors found in close proximity to any learned pattern.

3.6.3 Quantitative Metrics

Based on the above classifications, we computed the following quantitative metrics, which are averaged over all trials and all master seeds for each experimental condition:

- *Target Recall Rate*: The proportion of trials classified as *Target Pattern*. This metric quantifies the effective size of an attractor's basin of attraction.

- *Other Learned Recall Rate*: The proportion of trials classified as *Other Learned Pattern*. This measures the rate of “mis-recall.”
- *Spurious Fixed Point Rate*: The proportion of trials classified as *Spurious Attractor* that converged to a fixed point.
- *Cycle Rate*: The proportion of trials that converged to a limit cycle with a period of 2 or more.
- *Not Converged Rate*: The proportion of trials that did not converge to either a fixed point or a limit cycle within the maximum number of steps.
- *Fixed Point Rate*: The proportion of trials that converged to any fixed point (including target, other learned, and spurious). This is equivalent to $1.0 - (\text{Cycle Rate} + \text{Not Converged Rate})$.
- *Average Steps to Converge*: The average number of update steps required to reach a fixed point or detect a cycle, averaged only over the trials that converged.

4. Results

In this section, we present the results of our extensive numerical simulations. All plotted data points represent the mean values averaged across five master random seeds, and the shaded regions or error bars indicate the 95% confidence intervals, ensuring statistical robustness of our findings.

A foundational aspect of the network’s dynamics is its convergence behavior. While a formal proof of convergence for KLR-trained Hopfield networks with synchronous updates is not established, our experiments revealed a remarkable degree of stability. Across the tens of thousands of recall trials conducted for this study, every single trial converged to a stable state (either a fixed point or a limit cycle) within the maximum of 30 update steps.

Furthermore, a detailed analysis of non-stationary dynamics showed that the rate of convergence to limit cycles (*Cycle Rate*) was negligible ($< 0.1\%$) across all tested parameter regimes (see Appendix C for a representative plot). This empirical observation that the dynamics are overwhelmingly dominated by convergence to fixed points validates our subsequent focus on the analysis of these fixed point attractors and their properties.

4.1 Performance and Attractor Landscape Characteristics ($N = 500$)

First and foremost, the KLR-trained network demonstrates exceptional storage capacity and robustness, as shown in Fig. 1(a). For initial states with low noise (initial similarity ≥ 0.9), the network achieves near-perfect recall (*Target Recall Rate* ≈ 1.0) across the entire tested range, up to a remarkable storage load of $P/N = 4.0$. This performance vastly surpasses the classical Hebbian limit (≈ 0.14). The plot also illustrates a graceful degradation of performance as the initial noise increases; for instance, at a moderate noise level (initial similarity = 0.6), the network maintains high performance up to $P/N \approx 2.0$ before the recall rate begins to decline. This confirms the model’s dual strengths in both capacity and robustness.

To understand the nature of the recall failures observed at high loads and noise levels, we decomposed the errors into their constituent sources. The results, shown in Fig. 1(b), reveal a crucial the detailed breakdown of recall failures. At low to medium storage loads ($P/N < 1.5$), the rate of convergence to spurious attractors (*Spurious Error*, green lines) is negligible. In this regime, the dominant source of error is the convergence to an incorrect but valid learned pattern (*Other Learned Error*, orange lines). This “mis-recall” indicates that the basins of attraction for different stored patterns are competing with each other. However, a distinct behavior emerges at very high storage loads ($P/N > 2.0$) under high noise conditions (initial similarity < 0.2). As the storage load increases further, the rate of mis-recall to other learned patterns decreases, while the rate of convergence to spurious attractors sharply increases, eventually becoming the dominant failure mode. This suggests that in the extremely overloaded regime, the energy landscape becomes so rugged that the system frequently gets trapped in local minima (spurious states) that do not correspond to any stored memory, rather than being attracted to a wrong memory. It is important to note that for lower noise levels (e.g., initial similarity ≥ 0.4), the Spurious Error remains low even at high loads, confirming the robustness of the model within a reasonable operating range.

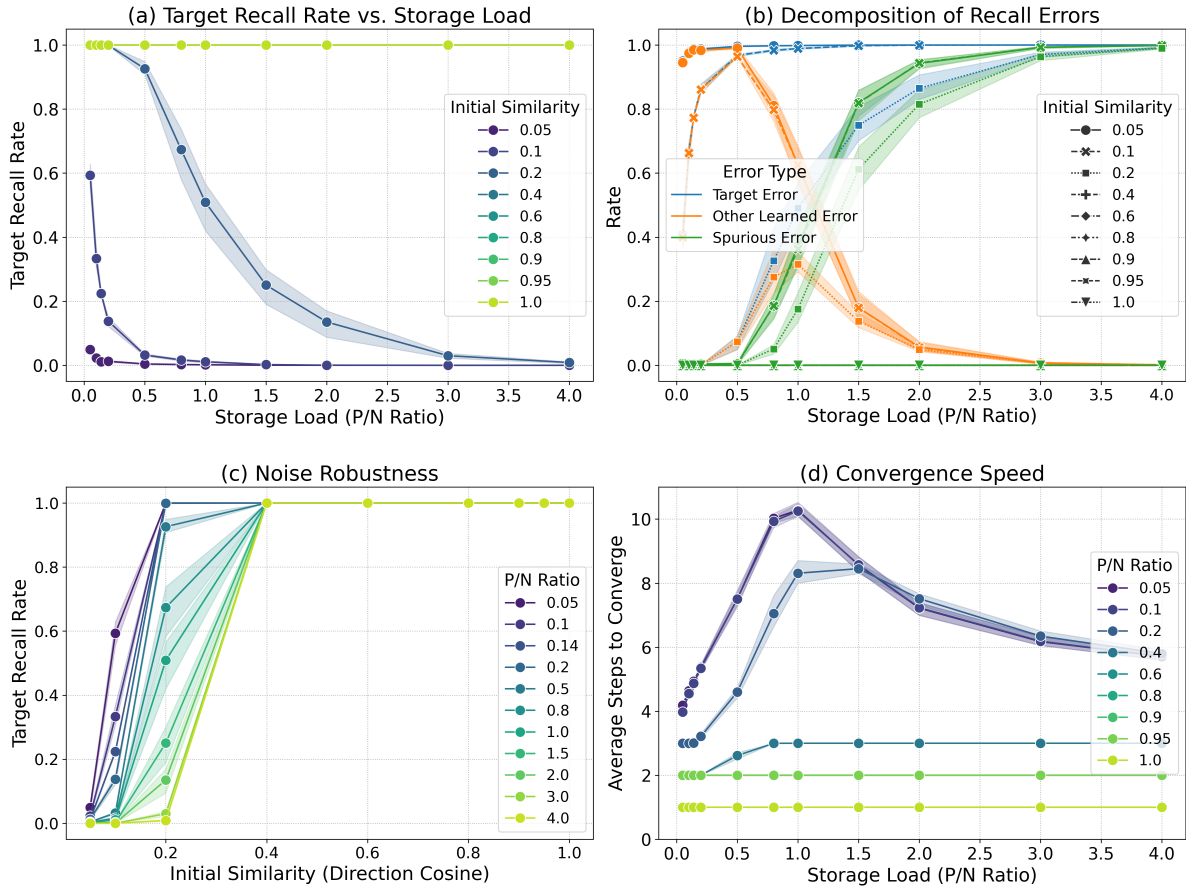


Fig. 1. Performance and attractor landscape characteristics of the KLR-trained network ($N = 500$). All curves show the mean values averaged across five master random seeds, with shaded regions representing the 95% confidence intervals. (a) **Capacity Curve:** *Target Recall Rate* as a function of storage load (P/N) for various initial similarities. The network maintains near-perfect recall up to $P/N = 4.0$ for low-noise inputs. (b) **Decomposition of Recall Errors:** Recall Errors ($1.0 - \text{Target Recall Rate}$) are decomposed into convergence to other learned patterns and spurious attractors. Colors distinguish the error type, while line styles represent different initial similarities. For moderate noise levels, the rate of spurious errors is negligible, demonstrating a remarkably clean landscape where mis-recall to other learned patterns is the dominant failure mode. However, under extreme conditions (high load and high noise), spurious errors become significant. (c) **Noise Robustness:** *Target Recall Rate* as a function of initial similarity for various storage loads (P/N). At low loads, recall is robust even from highly corrupted states. (d) **Convergence Speed:** Average number of steps to convergence for various initial similarities. Recall is exceptionally fast, typically within 1-2 steps for high-similarity inputs and well under 10 steps even for noisy, high-load conditions.

The network’s robustness to noise is further detailed in Fig. 1(c). This plot shows that at low storage loads (e.g., $P/N \leq 1.0$), the network is highly robust, capable of perfect recall even from initial states with similarities as low as 0.4. As the load increases, the recall process requires a higher initial similarity, signifying a shrinkage of the basins of attraction. The sharp, cliff-like transitions observed for each load level indicate that the basins of attraction are well-defined.

Finally, the recall dynamics are exceptionally fast, as illustrated in Fig. 1(d). For high-similarity initial states, the network consistently converges in only one or two steps. Even for highly corrupted states in the low-similarity regime, the average number of steps to convergence remains remarkably small, typically well below 10 steps. Notably, for these noisy inputs, the convergence time exhibits a non-monotonic “hump” shape, peaking at intermediate storage loads. The subsequent decrease in convergence time at very high loads corresponds precisely to the regime where recall failures dominate (cf. Fig. 1(b)).

This observation suggests that the dynamics rapidly settle into nearby stable states, which correspond to incorrect learned patterns or spurious fixed points, rather than conducting a prolonged search for the correct

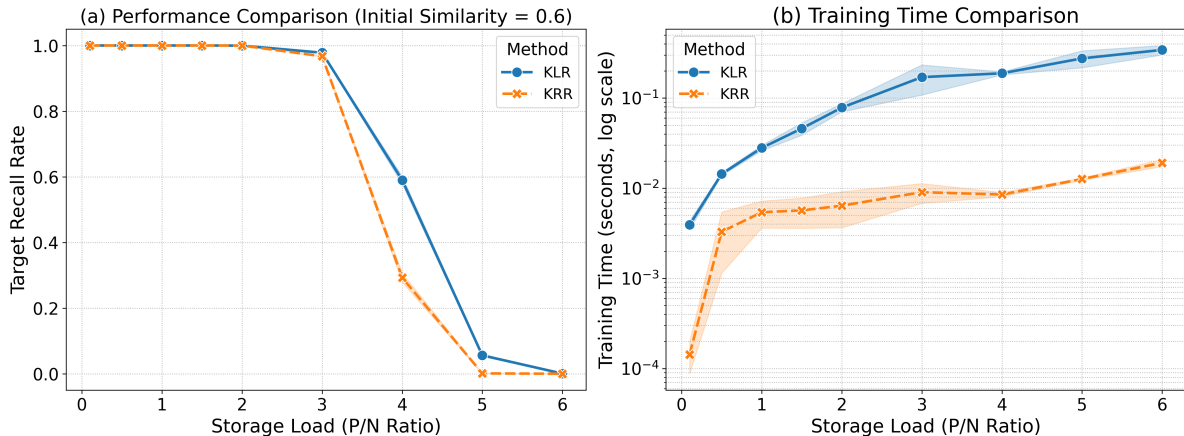


Fig. 2. Comparative analysis of Kernel Logistic Regression (KLR) and Kernel Ridge Regression (KRR) for a network with $N = 100$ neurons and an optimized kernel width ($\gamma = 0.02$). All curves show the mean over five master seeds, with shaded regions representing the 95% confidence intervals (for performance) or standard deviation (for timing). (a) **Performance Comparison:** *Target Recall Rate* as a function of storage load (P/N) under a moderate noise condition (initial similarity = 0.6). Both methods exhibit high and qualitatively similar performance, maintaining near-perfect recall up to $P/N \approx 3.0$. (b) **Training Time Comparison:** Training time in seconds (log scale) as a function of storage load. The non-iterative, closed-form solution of KRR results in a training process that is consistently one to two orders of magnitude faster than the iterative gradient descent required for KLR.

target. Such rapid convergence represents a meaningful practical advantage of the model.

4.2 Comparison with Kernel Ridge Regression ($N = 100$)

To contextualize the properties of the KLR-trained network and address the question of whether its high performance is a unique feature of the logistic loss function, we conducted a direct comparative analysis against Kernel Ridge Regression (KRR). KRR offers an alternative kernel-based learning framework that minimizes squared error loss and, crucially, admits a non-iterative, closed-form solution. The comparison was performed on a network of $N = 100$ neurons using the empirically determined optimal kernel width ($\gamma = 0.02$) for this scale.

The results of this comparison are summarized in Fig. 2. We first evaluated the recall performance under a moderate noise condition (initial similarity = 0.6), as shown in Fig. 2(a). The performance of the two methods is remarkably similar. Both KLR and KRR maintain near-perfect recall for storage loads up to $P/N \approx 3.0$. Beyond this critical capacity, both methods exhibit a sharp yet smooth degradation in performance, with their recall curves closely aligned. Although minor quantitative differences exist, with KLR displaying a slightly wider shoulder in this case, the overall qualitative behavior is essentially identical. These findings strongly suggest that the observed high-capacity and robust attractor dynamics are not specific to KLR but are likely a more general property of Hopfield-type networks trained with kernel regression methods that effectively separate patterns in a high-dimensional feature space.

In stark contrast to their performance similarity, the two methods exhibit a dramatic difference in computational efficiency for training. Fig. 2(b) plots the training time as a function of storage load. The non-iterative nature of KRR provides a substantial advantage: its training process is consistently one to two orders of magnitude faster than the iterative gradient descent required for KLR across the entire range of storage loads. For instance, at $P/N = 4.0$, KRR training completes in approximately 0.01 seconds, whereas KLR requires over 1 second. This difference in efficiency grows with the number of patterns, highlighting KRR as a highly attractive and practical alternative for training large-scale associative memories.

In summary, this comparative analysis clarifies the trade-offs between KLR and KRR. While both methods can construct similarly high-performance attractor landscapes, KRR achieves this with significantly lower computational cost for training. This reinforces the generality of our findings while also providing important practical insights for future implementations. It is important to note, however, that this computational advantage applies only to the training phase. The recall process for both KLR and KRR requires the evaluation of kernel

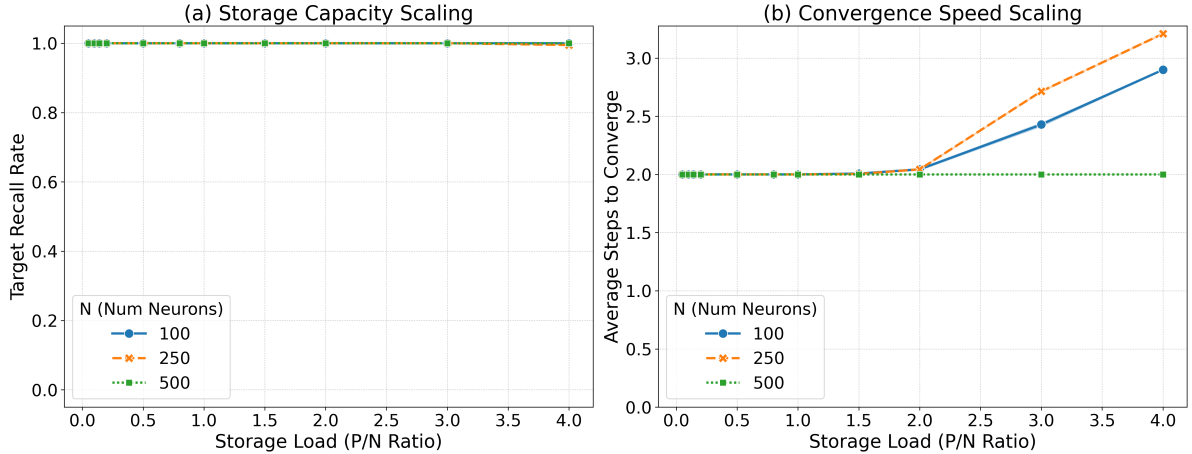


Fig. 3. Scaling analysis of storage capacity and convergence dynamics under N -dependent optimal kernel widths (γ_{opt}). The analysis was performed under a moderate noise condition (Initial Similarity = 0.8) for three different network sizes: $N = 100, 250$, and 500 . (a) **Storage Capacity Scaling:** The *Target Recall Rate* curves for all three network sizes largely collapse onto a single curve, particularly in the high-performance regime ($P/N \lesssim 3.5$). While minor deviations are observed at the highest loads, this trend provides strong evidence that the storage capacity P scales linearly with the network size N . (b) **Convergence Speed Scaling:** In contrast, the convergence dynamics exhibit a clear dependence on the absolute network size. For a given P/N ratio in the high-load regime, larger networks converge significantly faster. This suggests that while the stability of attractors is governed by relative load, the efficiency of the recall dynamics is enhanced in higher-dimensional state spaces.

similarities between the current state and all P stored patterns at each update step, resulting in a computational complexity of $O(NP)$ per step. This contrasts with the $O(N^2)$ complexity of traditional Hopfield networks and can become a bottleneck in systems with a very large number of stored patterns ($P \gg N$). Exploring efficient kernel approximation methods to mitigate this recall complexity remains an important direction for future work.

4.3 Scaling Analysis of Storage Capacity and Dynamics

A critical question for any associative memory model is how its storage capacity scales with the network size, N . To address this and verify that our findings are not artifacts of a specific network size, we conducted a scaling analysis for networks of $N = 100, 250$, and 500 neurons.

During our initial investigation, a naive application of the conventional kernel scaling rule, $\gamma = 1/N$, led to the counter-intuitive result that the storage capacity coefficient P/N decreased for larger networks. This motivated a focused analysis of the interplay between N and γ . We found that the optimal kernel width, γ_{opt} , which maximizes recall performance at high loads, exhibits a non-trivial dependence on the network size. Specifically, our empirical analysis revealed that larger networks require a more localized kernel to achieve maximum capacity, with the optimal scaling factor $c_{\text{opt}} = \gamma_{\text{opt}}N$ increasing with N (e.g., $c_{\text{opt}} \approx 2$ for $N \leq 250$ and $c_{\text{opt}} \approx 5$ for $N = 500$). A detailed account of this hyperparameter optimization is provided in Section 4.4.

Armed with this crucial insight, we re-evaluated the scaling law using the empirically determined, N -dependent optimal gamma values for each network size. The results, performed under a moderate noise condition (Initial Similarity = 0.8), are presented in Fig. 3.

As shown in Fig. 3(a), the Target Recall Rate curves for all three network sizes now largely collapse onto a single curve, particularly in the high-performance regime. While minor deviations are observed at very high loads (e.g., $P/N = 4.0$), the performance is predominantly determined by the relative storage load P/N , irrespective of the absolute network size N . This result provides strong evidence that, under appropriately scaled kernel parameters, the storage capacity of the KLR-trained network follows the fundamental linear scaling law, $P \propto N$. This confirms that the high capacity coefficients reported are a general property of the model and not a finite-size effect.

Interestingly, while the static property of storage capacity follows a simple P/N scaling, the temporal dynamics of the recall process exhibit a more complex, scale-dependent behavior. Fig. 3(b) plots the average

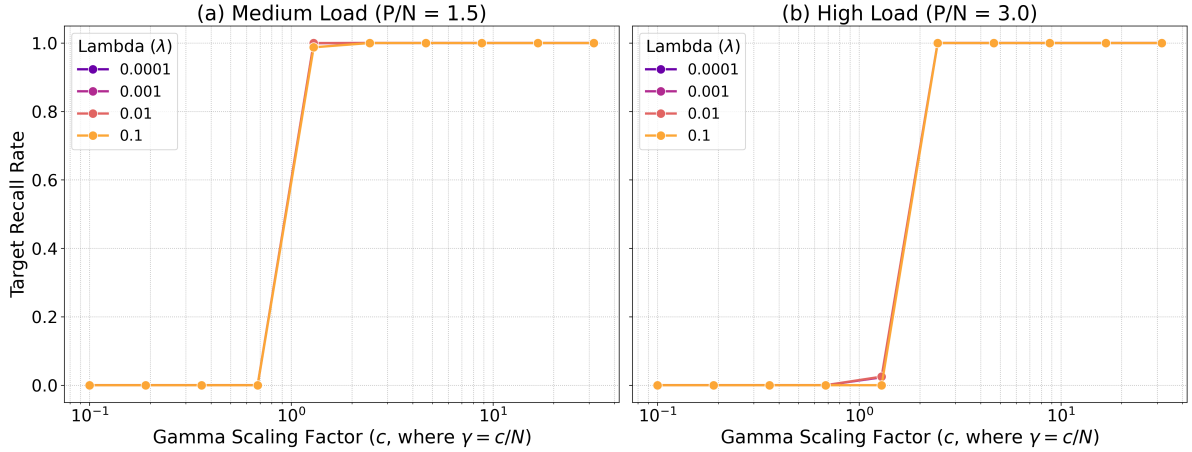


Fig. 4. Hyperparameter sensitivity analysis for a network with $N = 100$ neurons. The plots show the Target Recall Rate as a function of the scaling factor c (where $\gamma = c/N$), for four different values of the L2-regularization parameter λ . All data points are averaged over five master seeds under a moderate noise condition (Initial Similarity = 0.8). (a) Performance at a medium storage load ($P/N = 1.5$). (b) Performance at a high storage load ($P/N = 3.0$). The results reveal a sharp phase transition, indicating that a minimum level of kernel locality ($c \gtrsim 1$) is required for successful recall. Crucially, the performance is remarkably robust to the choice of λ over several orders of magnitude, as the curves for different λ values are nearly indistinguishable.

number of steps to convergence. In contrast to the performance curves, the convergence speed does not collapse onto a single curve. For any given P/N ratio in the high-load regime, larger networks converge significantly faster than smaller ones. For example, at $P/N = 4.0$, the $N = 500$ network converges in approximately 2 steps, whereas the $N = 100$ network requires nearly 3 steps.

This dissociation between the scaling of capacity and the scaling of convergence speed is a non-trivial finding. It suggests that while the existence and size of the basins of attraction are governed by the relative density of patterns (P/N), the efficiency of the trajectory towards the attractor’s center is enhanced in higher-dimensional state spaces. This intriguing scale-dependent acceleration of dynamics will be further explored in the Discussion section.

4.4 Hyperparameter Sensitivity

Finally, we investigated the sensitivity of the network’s performance to its two key hyperparameters: the kernel width γ (parameterized by the scaling factor $c = \gamma N$) and the L2-regularization parameter λ . A robust performance across a reasonable range of these parameters is crucial for the practical applicability of the model. We performed a systematic sweep of c and λ for a network of $N = 100$ under both medium ($P/N = 1.5$) and high ($P/N = 3.0$) storage loads.

The results are presented in Fig. 4. The plots reveal two fundamental characteristics of the KLR-trained network. First, the network’s performance exhibits a sharp phase transition with respect to the kernel locality c . For both medium and high load conditions, the *Target Recall Rate* is near zero for small c values ($c < 1$) and abruptly jumps to near-perfect recall once c crosses a critical threshold. This indicates that a minimum level of kernel locality is essential for the learning algorithm to successfully form distinct, stable attractors. Interestingly, the critical threshold for c appears to be slightly larger for the high-load case (Fig. 4(b)) than for the medium-load case (Fig. 4(a)), corroborating our earlier finding that higher memory congestion requires a more localized kernel to mitigate inter-pattern interference. Second, and most strikingly, the network’s performance is remarkably robust to the choice of the regularization parameter λ . As shown in both plots, the performance curves for four different λ values, spanning three orders of magnitude (from 0.0001 to 0.1), are nearly indistinguishable from one another. This result is of significant practical importance, as it suggests that the KLR Hopfield network does not require meticulous fine-tuning of the regularization parameter to achieve high performance. The learning mechanism appears to be inherently stable and capable of finding effective solutions across a very broad range of λ .

In summary, this sensitivity analysis demonstrates that while the kernel width γ is a critical parameter that must be chosen to ensure sufficient kernel locality (i.e., $c = \gamma N$ must be large enough), the model is exceptionally robust with respect to the regularization parameter λ . This provides a clear and practical guideline for the design and application of KLR-trained associative memories.

5. Discussion

Our extensive quantitative analysis has provided a comprehensive picture of the attractor landscape in KLR-trained Hopfield networks. A central finding is the emergence of a remarkably “clean” landscape, characterized by a near-zero rate of spurious fixed points, particularly under high storage loads with moderate noise (Fig. 1(b)). This strong suppression of spurious states is a key factor behind the model’s high fidelity. But what is the mechanism behind this suppression?

We hypothesize that two aspects of KLR learning are crucial. First, the kernel trick implicitly maps the input patterns into a high-dimensional feature space where they become more easily separable [6]. This enhanced separability allows the learning algorithm to find decision boundaries that create wide, well-defined basins of attraction for the stored patterns, effectively pushing potential spurious minima away from the recall trajectories. Second, the logistic loss function, combined with L2-regularization, encourages the formation of a “smooth” energy landscape. This property is akin to the margin maximization in SVMs; by pushing the decision boundaries away from the data points, the learning process effectively deepens the basins of attraction around the stored patterns. Unlike Hebbian learning, which is based on simple pairwise correlations and can create many noisy local minima, the KLR objective seeks a solution with a large margin, which tends to flatten the landscape in regions far from the decision boundaries. This landscape smoothing further inhibits the formation of unintended spurious attractors. A detailed theoretical investigation of this mechanism is the subject of our companion paper [12].

Generality of High-Capacity Kernel-Based Memories: Our direct comparison between KLR and KRR (Fig. 2) yields a crucial insight: the remarkable ability to form a clean, high-capacity attractor landscape is not a feature unique to the logistic loss function of KLR. The qualitatively similar performance of KRR suggests that this is a more general property of kernel regression methods applied to Hopfield-type networks. The key mechanism appears to be the kernel trick itself, which maps patterns into a high-dimensional feature space where they become more easily separable, allowing the learning algorithm to sculpt well-defined attractor basins.

Theoretically, this similarity is further supported by the connection between the two algorithms. It is well-established that the optimization of the KLR objective via Newton’s method (Iteratively Reweighted Least Squares) is mathematically equivalent to solving a sequence of weighted Kernel Ridge Regression problems [13–15]. In this view, KLR is an iteratively refined version of KRR that focuses on difficult patterns. The fact that standard KRR performs comparably suggests that for the random patterns used in this study, such iterative refinement yields only marginal gains. While their performance is similar, the significant computational advantage of KRR’s non-iterative solution makes it a compelling practical alternative, highlighting a clear trade-off between algorithmic approaches.

The Non-Trivial Scaling of Stability: The scaling analysis (Fig. 3) revealed one of the most profound findings of this study: the relationship between network size N and the optimal kernel width γ is non-trivial. Contrary to the conventional $\gamma = 1/N$ rule of thumb, we found that maintaining optimal storage capacity requires γ to be scaled such that the factor $c = \gamma N$ increases with N . This indicates that larger networks necessitate more localized kernels to effectively manage the increasingly complex web of inter-pattern interactions in a high-dimensional state space. In essence, as the memory space becomes more crowded with patterns in a higher-dimensional state space, each stored memory must become more “introverted,” narrowing its field of influence to avoid interfering with its neighbors. This scale-dependent requirement for locality is a new, fundamental principle for designing high-capacity kernel-based associative memories. The requirement for locality can also be interpreted as a means to maintain the effective rank of the kernel matrix high enough to ensure linear separability in the high-dimensional feature space. As a practical guideline derived from our findings, optimal performance for random patterns can be achieved by selecting γ such that the scaling factor $c = \gamma N$ is in the range of approximately 2 to 5. Once this principle is respected, we confirmed that the storage capacity follows the expected linear scaling law, $P \propto N$, demonstrating the model’s soundness as a scalable

architecture.

Dissociation of Performance and Dynamics Scaling: Intriguingly, while storage capacity (a static property) scales with the relative load P/N , the recall dynamics (a temporal property) do not. As shown in Fig. 3(b), for a given P/N , larger networks converge significantly faster. This dissociation suggests that the geometry of the attractor landscape changes with N in a subtle way. We hypothesize that in higher-dimensional state spaces, the energy landscape becomes “smoother” or less rugged, allowing the state to follow a more direct path to the attractor minimum. This “blessing of dimensionality” for dynamics, coexisting with a simple P/N scaling for capacity, is a fascinating aspect of this system that warrants further theoretical investigation.

Robustness and Practical Implications: Our hyperparameter sensitivity analysis (Fig. 4) provided both a theoretical insight and a practical guideline. The sharp phase transition with respect to the kernel locality c underscores its criticality: a minimum level of locality is non-negotiable for stability. Conversely, the astonishing robustness of performance to the regularization parameter λ over several orders of magnitude is a highly desirable feature. It implies that, once the kernel is appropriately scaled, the system is remarkably stable and does not require meticulous fine-tuning, greatly enhancing its practical applicability.

In conclusion, this work has moved the understanding of KLR-trained Hopfield networks from a collection of performance benchmarks to a well-characterized dynamical system. By revealing the generality of the approach (via KRR comparison), the non-trivial scaling laws of its parameters, and the robust nature of its performance, we have established a solid foundation for both the theoretical exploration and practical engineering of the next generation of high-capacity, brain-inspired associative memories.

6. Conclusion

In this paper, we presented a comprehensive quantitative analysis of the attractor landscape in Hopfield networks trained with Kernel Logistic Regression, addressing critical questions regarding the model’s performance, generality, and scalability. Through a series of rigorous, statistically validated simulations, we have moved beyond the initial discovery of high capacity to establish a deeper, more principled understanding of this powerful associative memory system.

Our findings confirm that KLR training sculpts a remarkably clean and robust attractor landscape, characterized by a near-zero rate of spurious states across a broad range of parameters and exceptionally fast recall dynamics. Our comparative analysis revealed that this high performance is a general feature of kernel regression methods, though KLR and KRR present a trade-off between iterative flexibility and closed-form efficiency.

Most significantly, we uncovered a non-trivial, scale-dependent scaling law for the kernel width, demonstrating that optimal storage capacity is intrinsically linked to the appropriate tuning of the kernel’s locality with network size. Under this optimized scaling, we provided definitive evidence that the storage capacity scales linearly with network size, $P \propto N$, solidifying the model’s foundation as a scalable architecture. Furthermore, we demonstrated the model’s practical robustness, showing its high performance to be remarkably insensitive to the choice of the regularization parameter.

In summary, this work provides a clear set of empirical findings and practical design principles for constructing high-capacity, kernel-based Hopfield networks. By systematically characterizing the properties of the attractor landscape and its dependence on key parameters, we have laid a solid foundation for future theoretical work and explorations into alternative loss functions, such as hinge loss for sparsity-induced efficiency. This establishes a robust framework for the engineering of next-generation, brain-inspired memory systems.

Funding

Not applicable.

Conflicts of interest

The authors declare no competing interests.

Author contribution

All the authors contributed equally to the present work.

Artificial intelligence tools

We used Gemini 2.5 Pro and ChatGPT (GPT-5.1) for proofreading the English manuscript.

References

- [1] J.J. Hopfield, “Neural networks and physical systems with emergent collective computational abilities.,” *Proceedings of the National Academy of Sciences*, vol.79, no.8, pp.2554–2558, 1982.
- [2] D.J. Amit, H. Gutfreund, and H. Sompolinsky, “Storing infinite numbers of patterns in a spin-glass model of neural networks,” *Phys. Rev. Lett.*, vol.55, pp.1530–1533, 1985.
- [3] D.J. Amit, H. Gutfreund, and H. Sompolinsky, “Spin-glass models of neural networks,” *Phys. Rev. A*, vol.32, pp.1007–1018, 1985.
- [4] T. Kohonen, *Self-organization and associative memory: 3rd edition*, Springer-Verlag, Berlin, Heidelberg, 1989.
- [5] D.J.C. MacKay, *Information theory, inference & learning algorithms*, Cambridge University Press, USA, 2002.
- [6] B. Scholkopf and A.J. Smola, *Learning with kernels: support vector machines, regularization, optimization, and beyond*, MIT Press, Cambridge, MA, USA, 2001.
- [7] A. Tamamori, “Kernel logistic regression learning for high-capacity hopfield networks,” *IEICE Transactions on Information and Systems*, vol. E.109-E, no. 2, 2026 (in press).
- [8] A. Tamamori, “Kernel ridge regression for efficient learning of high-capacity hopfield networks,” *Proceedings of Asia-Pacific Signal and Information Processing Association Annual Summit Conference (APSIPA ASC)*, 2025.
- [9] D. Nowicki and H. Siegelmann, “Flexible kernel memory,” *PLOS ONE*, vol.5, no.6, pp.1–18, 2010.
- [10] B. Caputo and H. Niemann, “Storage capacity of kernel associative memories,” *Proceedings of the International Conference on Artificial Neural Networks*, pp.51–56, 2002.
- [11] H. Ramsauer, B. Schäfläfl, J. Lehner, P. Seidl, M. Widrich, L. Gruber, M. Holzleitner, T. Adler, D. Kreil, M. Kopp, G. Klambauer, J. Brandstetter, and S. Hochreiter, “Hopfield network is all you need,” *Proceedings of International Conference on Learning Representations*, 2021.
- [12] A. Tamamori, “Self-organization of attractor landscapes in high-capacity kernel hopfield networks,” arXiv preprint, 2511.13053, 2025.
- [13] C. M. Bishop. “Pattern recognition and machine learning,” Springer, 2006.
- [14] C. E. Rasmussen and C. K. I. Williams, “Gaussian processes for machine learning,” MIT Press, 2006.
- [15] K. P. Murphy, “Probabilistic machine learning: an introduction,” MIT Press, 2022.

Appendix

A. Convergence of KLR Learning

To validate that the number of updates used for Kernel Logistic Regression (KLR) training was sufficient for the convergence of the model parameters, we analyzed the learning curve under a challenging, high-load condition. Fig. A-1 plots the total loss (negative log-likelihood plus L2-regularization term) as a function of the number of gradient descent updates for a network with $N = 500$ neurons and a storage load of $P/N = 4.0$.

As the figure illustrates, the loss decreases by several orders of magnitude within the initial 150 updates and visibly approaches a plateau. The rate of decrease becomes negligible towards the end of the 200-update training period. This confirms that 200 updates are adequate to achieve a well-converged model, ensuring that the performance results reported in the main text are not limited by incomplete training.

B. Validation of Attractor Classification

To validate the strict equality-based classification of attractors used in our study, we analyzed the distribution of Hamming distances between final states of failed recall trials and their nearest learned patterns. Fig. B-1 shows the histogram of these distances, separated by failure type (Other Learned vs. Spurious).

As expected, all trials classified as Other Learned resulted in final states with a Hamming distance of exactly 0 to a non-target learned pattern. Conversely, all trials classified as Spurious resulted in final states with a significant, non-zero Hamming distance to any of the learned patterns. The clear separation between these two

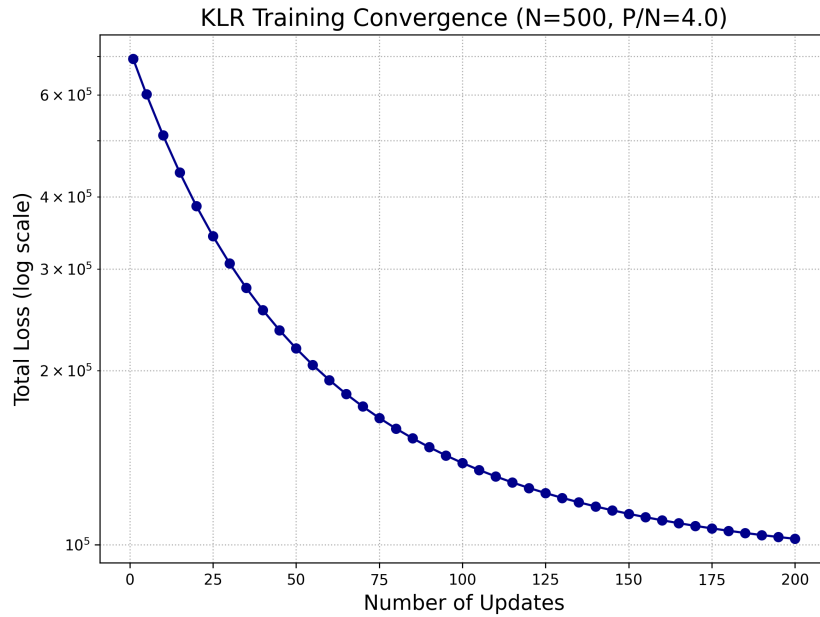


Fig. A-1. Training convergence of Kernel Logistic Regression (KLR). The plot shows the total loss as a function of the number of updates for a network under a high-load condition ($N = 500$, $P/N = 4.0$). The curve demonstrates that the loss effectively converges within the 200 updates used in our experiments.

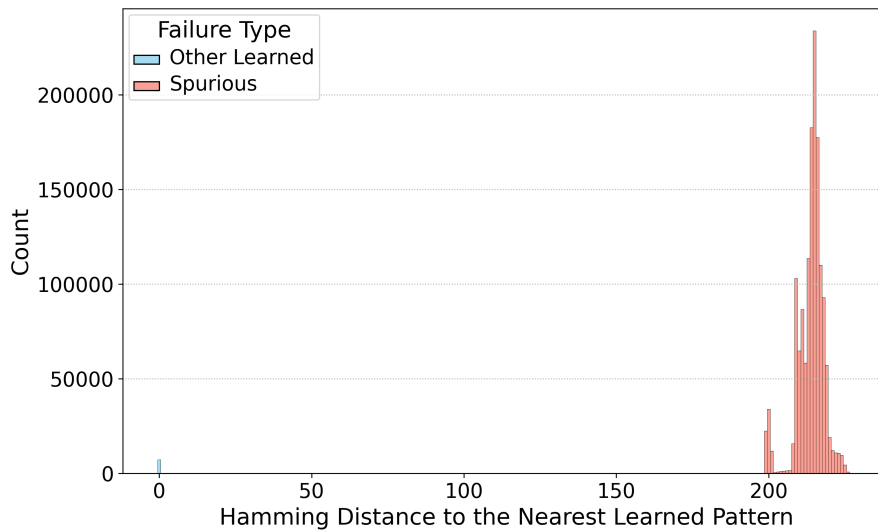


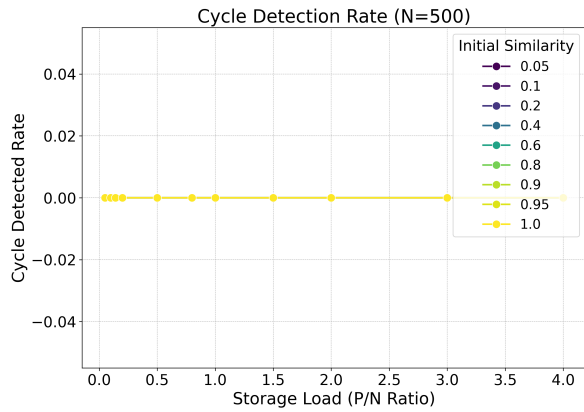
Fig. B-1. Histogram of the Hamming distance from the final state of a failed trial to the nearest learned pattern. The distribution is shown for trials classified as Other Learned (blue) and Spurious (red). The perfect separation of the two distributions validates our strict, equality-based classification criterion.

distributions, with no spurious attractors found in close proximity (e.g., Hamming distance < 10) to any learned pattern, confirms the validity of our classification methodology.

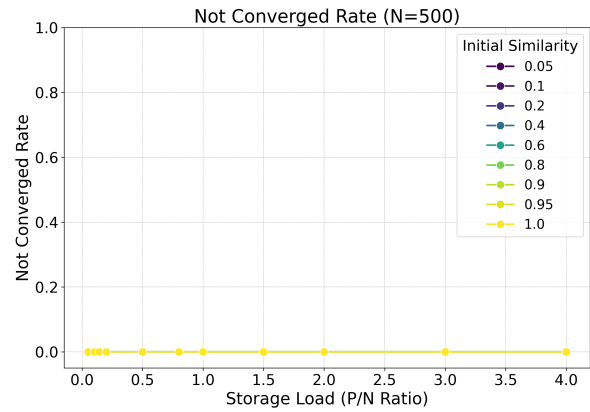
C. Analysis of Non-Stationary Dynamics

To ensure that our analysis, which primarily focuses on fixed point attractors, is not biased by the presence of other dynamical behaviors, we systematically quantified the rate of convergence to non-stationary states. This appendix presents the results for the rates of convergence to limit cycles and non-convergence within the maximum simulation steps.

Figure C-1 shows the *Cycle Rate* and the *Not Converged Rate* as a function of storage load (P/N) for a network of $N = 500$. As can be seen in Fig. C-1(a), the *Cycle Rate* is effectively zero across all tested



(a) Cycle Detection Rate vs. Storage Load



(b) Not Converged Rate vs. Storage Load

Fig. C-1. Analysis of non-stationary dynamics for $N = 500$. All data points represent the mean over five master seeds. Shaded regions indicate 95% confidence intervals, though they are mostly invisible as the rates are zero. (a) The proportion of trials that converged to a limit cycle. (b) The proportion of trials that did not converge within 30 steps. Both rates are effectively zero across all conditions, confirming that the network dynamics are dominated by convergence to fixed points.

conditions, with no trials converging to a limit cycle with a period of 2 or more. Similarly, Fig. C-1(b) shows that the *Not Converged Rate* is also zero, confirming that every recall trial reached a stable state (either a fixed point or a cycle) within the 30 update steps.

These results validate our focus on fixed point attractors, as they overwhelmingly dominate the dynamics of the KLR-trained network under the conditions studied in this paper.